Biochimica et Biophysica Acta 904 (1987) 346–352
Elsevier

BBA 73756

ESR imaging of myelin basic protein induced vesicle aggregation

T. Páli [a], B. Ebert [b] and L.I. Horváth [a]

[a] *Institute of Biophysics, Biological Research Center, Szeged (Hungary)* and [b] *Department of Biophysics, Central Institute of Molecular Biology, Berlin-Buch (G D R)*

(Received 13 April 1987)
(Revised manuscript received 18 August 1987)

Key words Lipid–protein interaction, Myelin basic protein, Spin labeling, ESR, Vesicle aggregation

Using a modulated magnetic field gradient technique, the conventional ESR spectrum of well-defined spatial sections and the one-dimensional-ESR image of the nitroxide centre line of spin-labeled stearic acid in phospholipid vesicles were recorded with a spatial resolution of $4 \cdot 10^{-5}$ m after pelleting the vesicles inside 1 mm (i.d.) sample capillaries in a slow centrifuge ($2500 \times g$). The sedimentation characteristics of dimyristoylphosphatidylcholine and dimyristoylphosphatidylglycerol vesicles were quantitatively compared with particular reference to vesicle aggregation induced by myelin basic protein. Protein-induced changes in the effective molecular mass were determined from ESR images of sedimentation profiles. The present data lend further support to the notion that the primary target of myelin basic protein–lipid interaction is the acidic lipid pool of myelin.

Introduction

The basic protein is known to have a key role in stabilizing the unique stacked lamellae of myelin sheaths in the central nervous system (for review see Ref. 1). As a peripheral protein, myelin basic protein interacts with the membrane interface mainly via electrostatic forces as demonstrated by biphasic solvent systems [2], monolayer [3], and light scattering experiments [4], and various spectroscopic studies [5–7] although shorter apolar sequences of the polypeptide chain should penetrate into the hydrophobic interior of the membrane [1,3,5,8]. Owing to its hairpin folding, myelin basic protein can very efficiently stack closely juxtaposed membrane surfaces Of the various phospholipids, myelin basic protein preferentially interacts with 25–30 mol/mol acidic lipids, like phosphatidylserine (PS) or phosphatidylglycerol, to neutralize its 27 unmasked basic residues [1,2,9–11].

When myelin basic protein is added to phospholipid vesicles the turbidity of the lipid suspension immediately increases, indicating myelin basic protein-induced vesicle aggregation [4]. Since changes in vesicle aggregation are best studied by hydrodynamic methods, we have developed an ESR imaging technique which is a combination of conventional spin-labeling and sedimentation equilibrium experiments. Briefly, the sample is prepared as usual in conventional spin-labeling ESR, then is introduced into sample tubes and pelleted down at low speed, and the concentration

Abbreviations DMPC, dimyristoylphosphatidylcholine, DMPG, dimyristoylphosphatidylglycerol, ESR, electron spin resonance, Hepes, *N*-(2-hydroxyethyl)piperazine-*N'*-2-ethanesulfonic acid, 16-SASL, 16-(4′,4′-dimethyloxazolidine-*N*-oxyl)stearic acid

Correspondence L I Horváth, Institute of Biophysics, Biological Research Center, P O B 521, H-6701 Szeged, Hungary

profile is recorded by one-dimensional ESR imaging. From the evaluation of such concentration profiles, quantitative data can be obtained on myelin basic protein-induced vesicle aggregation.

Materials and Methods

1,2-Dimyristoyl-*sn*-glycero-3-phosphorylcholine (DMPC) was obtained from Fluka (Buchs, Switzerland); 1,2-dimyristoyl-*sn*-glycero-3-phosphorylglycerol (DMPG) was provided by Dr. D. Marsh (Göttingen, FRG). Both lipids gave single spots by thin-layer chromatography and were used without further purification. The C-16 positional isomer of spin-labeled stearic acid (16-SASL) was obtained from Aldrich Chemical Co. (Beerse, Belgium). Myelin basic protein was provided by Dr. G.J. Tigyi of this Institute [12].

Lipid and 1 mol% spin probe were mixed in chloroform/methanol, evaporated to dryness by flowing N_2 gas, evacuated to remove solvent traces, and hydrated in 2 mM Hepes/1 mM EDTA (pH 7.4) buffer solution at a final concentration of 12 mg/ml. Myelin basic protein was dissolved in the same buffer and added to the lipid either with the hydrating solution or after lipid hydration. The myelin basic protein/lipid ratio was 1 : 85 mol/mol which, assuming uniform distribution, corresponds to a vesicle surface coverage of 32%. 0.1 ml aliquots of protein/lipid complexes were filled into sample capillaries (i.d. 1 mm) and centrifuged in a swing-out rotor at 4000 rpm (2500 $\times g$ at the bottom of the capillary, $l = 10$ cm) for 10 minutes. Since such capillaries are too long for X-band ESR spectrometers, the capillaries were cut into 9 mm pieces immediately after pelleting and closed with a small amount of clay which gave no disturbing signal in the nitroxide spectral region. No changes in one-dimensional ESR profiles were evident within 2–3 h of centrifugation.

Conventional ESR spectra were recorded with an ERS 220 X-band spectrometer (ZWG Berlin, G.D.R.) using a nitrogen gas flow variable temperature accessory (Varian, Switzerland). One-dimensional ESR imaging spectroscopy was done as previously reported using a modulated magnetic field gradient technique in conjunction with a low-pass filter [13,14]. Sample capillaries were introduced via the top sample port and placed in two different positions: either (i) along the conventional x- or (ii) y-axis of the TE_{102} rectangular cavity [15]. In the latter geometry, the sample capillary is introduced into the cavity in a transverse position, and thus its maximum length is limited by the opening of the port (i.d., 11 mm) and cavity Q considerations. In imaging experiments, however, this geometry must be favored because the gradient field $G_z(t)$ is varied along the y-axis, and a further advantageous feature is that the H_1 field is homogeneous along the y-axis of the TE_{102} rectangular cavity, and so absorption data need not be corrected for H_1 field inhomogeneities. The conventional sample geometry (parallel to the x-axis) was only used during spectrometer calibration as described below.

The magnetic field gradient of our modified spectrometer was calibrated with a pair of parallel capillaries with their long axes at a distance of $\Delta l = 3.3 \pm 0.1$ mm. The pair of capillaries were filled with 80 mM ethanolic solution of 16-SASL and placed perpendicularly to the $G_z(t)$ field (along the x-axis of the TE_{102} rectangular cavity, cf. sample geometry shown in Fig. 2). The magnetic field gradient was measured by setting the sensitive z_0 plane to the geometric center of one of the capillaries and then determining the modulation line broadening of the exchange-narrowed nitroxide line of 16-SASL in the other capillary. From the spectral separation of the overmodulated sidebands a magnetic field gradient of $G_z = 3.43$ T/m was estimated; the spatial resolution of our imaging ESR spectrometer was thus at least $4 \cdot 10^{-5}$ m along the y-axis of the cavity.

Results and Discussion

In conventional spin-labeling ESR experiments the spatial distribution of line samples can be estimated with a resolution of only 2–4 mm; in practice, the sample capillary is adjusted such that its dense section is centered in the middle of the cavity where the incident microwave power (H_1) and the modulation field have their maxima. In ESR imaging experiments a steeply varying magnetic field (G_z) is superimposed on the conventional static magnetic field (B_0) so that the resonance condition is only fulfilled on the so-called

sensitive plane (z_0 plane); the z_0 plane is perpendicular to the collinear B_0 and G_z fields (for a review see Ref. 16). When using nitroxide spin probes, an additional difficulty arises due to the multiplet structure of the spectra, which is best overcome by a modulated magnetic field gradient $G_z(t)$ as previously demonstrated [14]. In this case, all species outside the sensitive z_0 plane are over-modulated and so the spectral contribution of an extremely small section of the sample (typically less than 0.1 mm) can selectively be detected. In our modified ZWG spectrometer, B_0 and $G_z(t)$ can independently be scanned and so either the conventional ESR spectrum of some well-defined spatial section or the spatial distribution of any ESR peak can be detected; in subsequent discus-

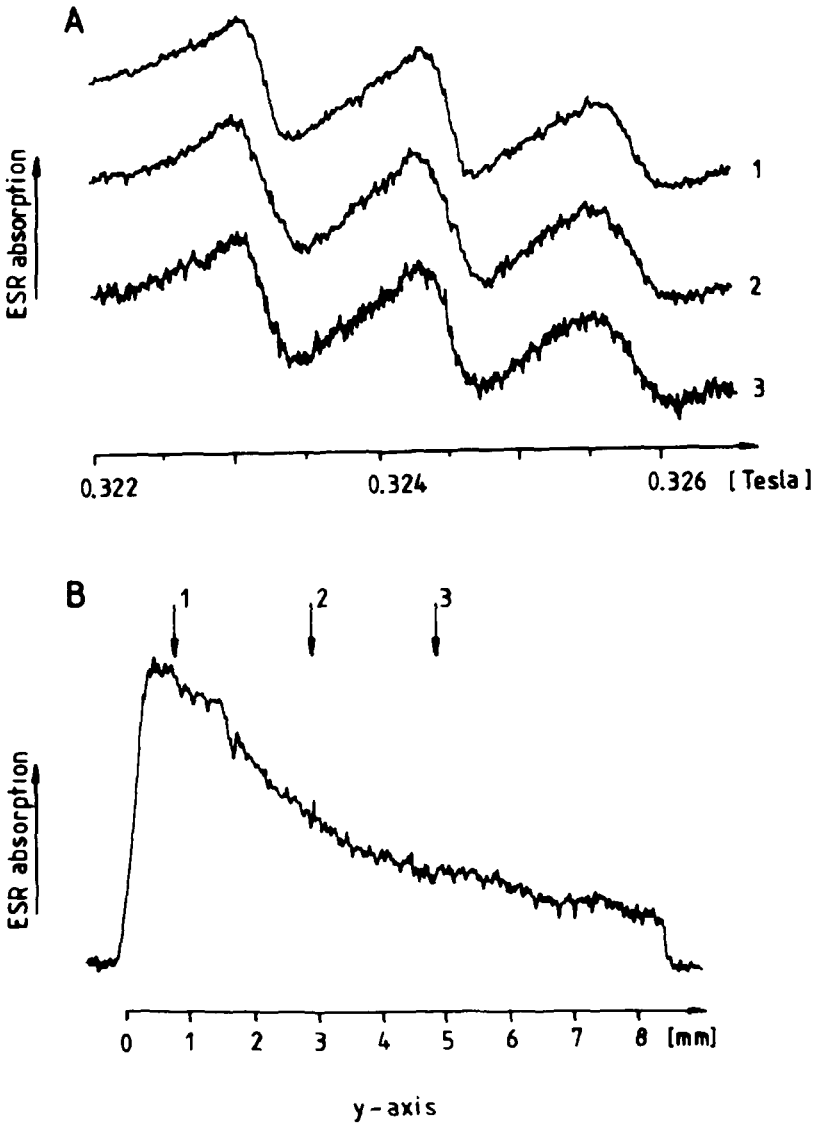

Fig 1 ESR spectra of pelleted spin-labeled DMPC vesicles in 1 mm (i d) sample capillaries in spectrum recording and image recording mode (A) Spatially selected ESR spectra of 16-SASL spin probe in spectrum recording mode at various positions along the sample capillary. (B) Spatial distribution of the nitroxide center line ($m_I = 0$) in the lower 9 mm segment of the sample capillary in image recording mode The one-dimensional ESR image was recorded with a modulated magnetic field gradient of $G_z = 3.43$ T/m corresponding to a spatial resolution of $4 \cdot 10^{-5}$ m For experimental details see Materials and Methods

sions we shall refer to these two operating modes as spectrum recording and image recording modes.

Spatially selected ESR spectra and the spatial distribution of the nitroxide center line ($m_I = 0$) are shown in Fig. 1. In this experiment spin labeled DMPC vesicles were pelletted in the 1 mm (i.d.) sample capillary at low rpm ($2500 \times g$). In the spectrum recording mode $G_z(t)$ was locked to different positions along the sample as indicated by arrowheads in Fig. 1B and the well-known nitroxide three-line pattern was recorded by scanning B_0; note the varying signal-to-noise ratios, which indicate spectral intensity differences (i.e., varying spin probe concentrations) in different sections. In the image recording mode, B_0 was locked to the nitroxide center line ($m_I = 0$), and $G_z(t)$ was scanned along a 9 mm section of the capillary. The sensitive z_0 plane is in practice a flat cylinder, the thickness of which is determined by the imaging resolution. Theoretically, the spatial resolution is given by

$$\Delta z = 0.67\ \Delta W_0 / G_z, \tag{1}$$

where ΔW_0 is the peak-to-peak linewidth of the nitroxide center line [12] in our case $\Delta W_0 = 2 \cdot 10^{-4}$ T and $G_z = 3.4 \pm 0.1$ T/m (see above), and so the spatial resolution was $4 \cdot 10^{-5}$ m along the y-axis of the cavity. However, it should be noted that the ESR absorption of the sensitive z_0 plane always has spurious contributions from nearby gradually overmodulated regions and, thus, sharp features (like edges or phase boundaries) will be blurred to some extent.

ESR imaging at X-band is severely limited by the size of the microwave cavity and so only small objects, typically less than 10 mm, can be investigated. Since our sample capillaries were too long

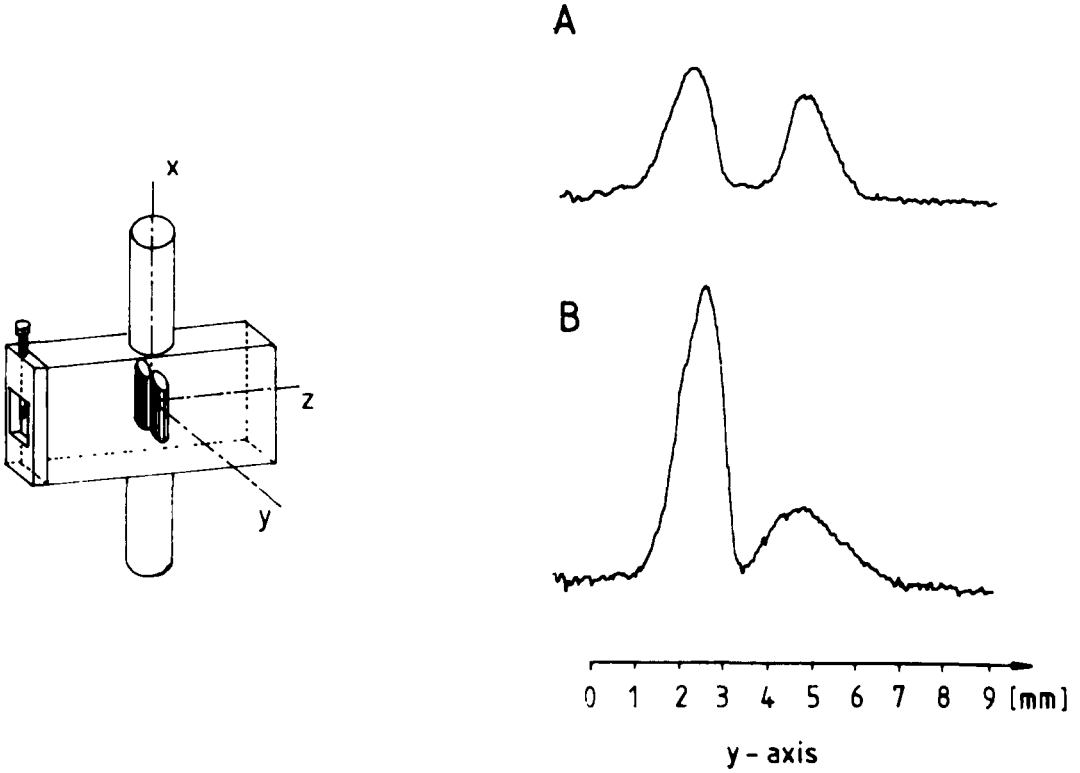

Fig 2 One-dimensional ESR image of the spatial distribution of pelleted spin-labeled DMPG vesicles in 1 mm (i d) sample capillaries (crosssectional projection). In these experiments the bottom and top 9 mm sections of the sample capillaries were placed perpendicularly to the modulated magnetic field $G_z(t)$ as shown in the inset (A) Pure DMPG vesicles in 2 mM Hepes/1 mM EDTA (pH 7 4), (B) DMPG/myelin basic protein complexes, lipid-to-protein ratio, 85 1 (mol/mol) For instrument settings see Fig 1

for ESR images along the capillary long axis with single image scans, an alternative method had to be developed to reach regions outside the 10 mm imaging scan range. This was particularly important for the quantitative analysis of DMPG sedimentation data, since pure DMPG hardly displayed a measurable concentration variation within 9 mm. Pure DMPC and DMPG are known to have the same thermal and acyl chain packing properties at neutral pH [17,18], but the size and the structure of their lipid headgroups are significantly different [19]; consequently the partial specific volume of DMPG is higher than that of DMPC. In addition DMPC vesicle preparations, unless purified by column chromatography, are prone to spontaneous aggregation into larger co-sedimenting multilayered structures and hence higher optical turbity and effective molecular mass can be observed [19]. The negatively charged DMPG vesicle preparations seem to be more homogeneous, although their size distribution was not measured.

In the subsequent experiments the capillaries were cut into 9 mm sections and the bottom and top 9 mm sections were placed next to each other perpendicular to the modulated magnetic field. (The very different spatial resolution along the x-axis should be noted; this was determined by the H_1-field profile along the x-axis [5].) As the sensitive z_0 plane was scanned (along the y-axis of the cavity) across the two capillary sections, two imaging peaks were observed, the ratio of

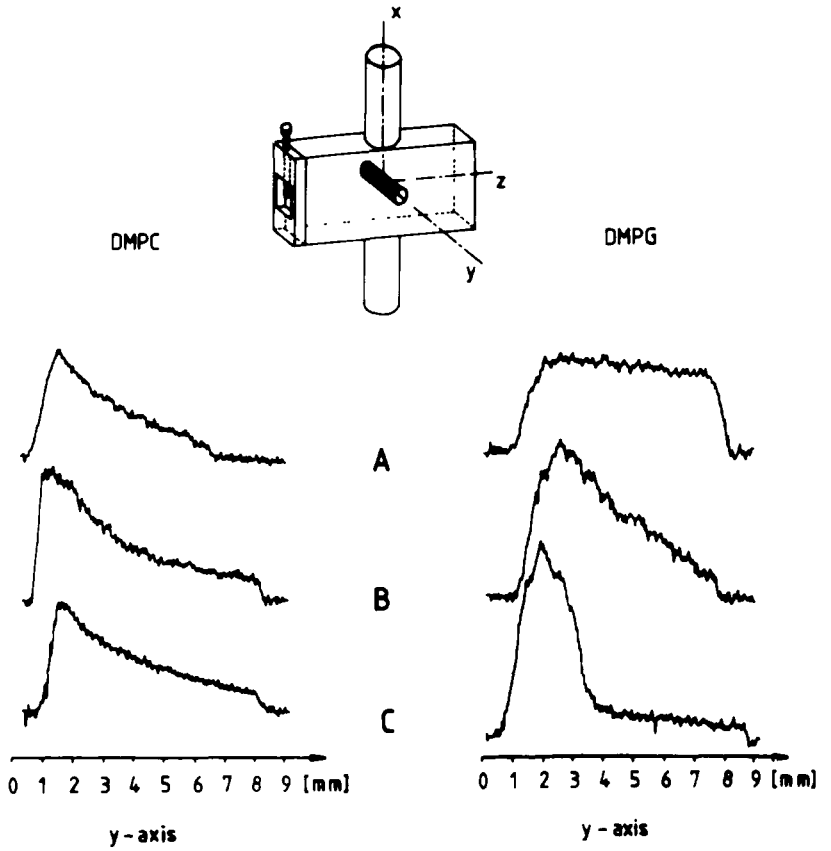

Fig 3 One-dimensional ESR image of the spatial distribution of pelleted spin-labeled DMPC and DMPG vesicles in 1 mm (i d) sample capillaries prior to (A) and after (B,C) the addition of myelin basic protein (projections along the capillary long axis) In these experiments, the bottom 9 mm sections of the sample capillaries were placed in parallel to the modulated magnetic field $G_z(t)$ as shown in the inset (A) Pure lipid vesicles preformed in buffer, (B) lipid vesicles hydrated with myelin basic protein-containing buffer, (C) preformed lipid vesicles (cf case (A)) after the addition of myelin basic protein-containing buffer For instrument settings see Fig 1

which depended on the average concentrations of the lipid vesicles in the two sections (Fig. 2).

Other projections (along the capillary long axis) of the spatial distribution of pelleted spin-labeled DMPG and DMPC vesicles in 1 mm (i.d.) sample capillaries are shown in Fig. 3. In these experiments the bottom 9 mm sections of the sample capillaries were placed in parallel to the modulated magnetic field gradient $G_z(t)$. Clearly, the DMPC image displays a sharp concentration gradient (Fig. 3A), the boundary region being spread out for only 6–8 mm; whereas the DMPG image was evenly spread out throughout the whole spatial section with very little or no decrease. The effect of myelin basic protein was studied by adding the protein to these lipids either with the hydrating buffer (Fig. 3B), or preformed vesicles were mixed with myelin basic protein-containing buffer (Fig. 3C). All the samples shown in Fig. 3 were pelleted simultaneously at approx. $2500 \times g$ for 10 min to ensure identical centrifugal forces. In the case of DMPC, which interacts with myelin basic protein only weakly [1,3–4], practically no change in the ESR image could be observed, but the ESR image of the sedimentation of DMPG vesicles changed entirely after the addition of myelin basic protein: in this case, the DMPG image displayed a short distorted plateau and a very sharp concentration gradient.

Multilamellar DMPC vesicles of large effective mass were rapidly depleted from the meniscus region and packed at the bottom with a sharp concentration gradient, whereas small unilamellar DMPG vesicles gave a smooth concentration gradient throughout the whole sample. The pelleting of lipid vesicles at low speed centrifugation is determined by sedimentation and diffusion; these two simultaneous effects will lead to exponentially decaying concentration gradients. From analysis of sedimentation profiles the effective mass can be calculated by measuring the ratio of concentrations c_1 and c_2 at radii r_1 and r_2,

$$M = \frac{2RT \ln(c_1/c_2)}{(r_1^2 - r_2^2)(1 - \rho v_s)\omega^2}, \qquad (2)$$

where ρ and v_s are the density and the partial specific volume of lipid vesicles at $T = 293$ K; ω, the angular velocity; R the gas constant. The ratio of concentrations can be read directly from the imaging traces shown in Fig. 3, since the H_1 field is homogeneous along the y-axis of the TE_{102} rectangular cavity; other parameters are constant. Since the angular velocity was not known with sufficient accuracy, all the samples were pelleted simultaneously to ensure identical conditions. The relative effective masses of DMPC vesicles prior to and after the addition of myelin basic protein remained virtually unaffected, whereas those of DMPG vesicles increased at least 170-fold after the addition of myelin basic protein. (It should be noted that the relative effective mass of pure DMPG vesicles was estimated from extended imaging scans, Fig. 2.) This change could be explained in two ways: (i) extensive vesicle aggregation with no size changes or (ii) myelin basic protein-induced fusion. In this latter case, small unilamellar DMPG vesicles are expected to fuse into large vesicles similarly to DMPC vesicles reported in Ref. 4. Qualitative analysis of electron micrographs were consistent with vesicle aggregation, but no large-scale fusion could be confirmed (Páli, T., Halász, N. and Horváth, L.I., unpublished results). Therefore, for the sake of simplicity, we assumed that the change in effective mass was entirely brought about by extensive vesicle aggregation, but the size and the average number of lipid molecules in DMPG vesicles were not affected by the adsorption of myelin basic protein

The physiological implications of myelin basic protein–lipid interaction are generally recognized [1,4]; our ESR imaging data lend support to the notion that the primary target of such interaction must be the acidic lipid pool of myelin. In the future, this imaging technique should be extended to salt-dependence studies and applied to other peripheral protein-lipid systems.

Acknowledgements

We gratefully thank Dr. D. Marsh (Göttingen, F.R.G.) for providing phosphatidylglycerol and Dr. G.J. Tigyi (this Institute) for purifying basic protein. One of us (T.P.) received a travel grant from the Hungarian Academy of Sciences.

References

1 Boggs, J M , Moscarello, M A and Papahadjopoulos, D (1982) in Lipid-Protein Interactions (Jost, P C and Griffith O.H. eds), Vol 2, pp 1–51, Academic Press, New York
2 Palmer, F B and Dawson, R M C (1969) Biochem J 111, 629–636
3 Demel, R A , London, Y , Geurts van Kessel, W S M , Vossenberg, F G A , and Van Deenen, L L M (1973) Biochim Biophys Acta 311, 507–519
4 Smith R (1977) Biochim Biophys Acta 470, 170–184
5 Boggs, J M and Moscarello, M A. (1978) J Membrane Biol 39, 75–96
6 Stollery, J G , Boggs, J.M , Moscarello, M A and Deber, C M (1980) Biochemistry 19, 2391–2396
7 Sixl, F , Brophy, P J and Watts, A (1984) Biochemistry 23, 2032–2039
8 London, Y , Demel, R A , Geurts van Kessel, W S M , Zahler, P and Van Deenen, L L M (1974) Biochim Biophys Acta 332, 69–84
9 Papahadjopoulos, D , Moscarello, M A , Eylar, E H and Isac, T (1975) Biochim Biophys Acta 401, 317–335
10 Boggs, J M , Moscarello, M A and Papahadjopoulos, D (1977) Biochemistry 16, 5420–5426
11 Boggs, J M., Wood, D.D and Moscarello, M.A (1980) Biochemistry 20, 1065–1073
12 Tigyi, G J , Balázs, L , Monostori, É and Andó, I (1984) Mol Immunol 21, 889–894
13 Karthe, W and Wehrsdorfer, E (1979) J Magn Reson 33, 107–111
14 Herrlig, T , Klimes, N , Karthe, W , Ewert, U and Ebert, B (1982) J Magn Reson 49, 203–211
15 Poole, C P (1967) Electron Spin Resonance, Ch 5, pp 112–182, Wiley Interscience, New York
16 Ohno, K (1986) Appl Spectr Rev 22, 1–56
17 Van Dijck, P W M , De Kruijff, B , Aarts, P A M M , Verkleij, A J , and De Gier, J (1978) Biochim Biophys Acta 506, 183–191
18 Browning, J L and Seeling, J (1980) Biochemistry 19, 1262–1270
19 Sixl, F and Watts, A (1982) Biochemistry 21, 6446–6452